www.sciencemag.org/cgi/content/full/327/5970/1254/DC1

Supporting Online Material for

RTEL-1 Enforces Meiotic Crossover Interference and Homeostasis

Jillian L. Youds, David G. Mets, Michael J. McIlwraith, Julie S. Martin, Jordan D. Ward, Nigel J. ONeil, Ann M. Rose, Stephen C. West, Barbara J. Meyer, Simon J. Boulton*

*To whom correspondence should be addressed. E-mail: simon.boulton@cancer.org.uk

Published 5 March 2010, *Science* **327**, 1254 (2010)
DOI: 10.1126/science.1183112

This PDF file includes

Supporting Online Material

RTEL-1 Enforces Meiotic Crossover Interference and Homeostasis

Jillian L. Youds, David G. Mets, Michael J. McIlwraith, Julie S. Martin, Jordan D. Ward, Nigel J. O'Neil, Ann M. Rose, Stephen C. West, Barbara J. Meyer & Simon J. Boulton*

*To whom correspondence should be addressed. E-mail: simon.boulton@cancer.org.uk

Materials and Methods

***C. elegans* strains.** Strains were cultured as described previously (*S1*). The strains used in this work include: FX1866 *rtel-1(tm1866)*, KR3499 *dpy-11(e224) unc-42(e270)*, KR342 *dpy-18(e364) unc-25(e265)*, KR180 *dpy-17(e164) unc-36(e251)*, DR181 *dpy-11(m35) unc-60(e224)*, KR1710 *unc-1(e719) dpy-7(sc27)*, CB4856 Hawaiian, TY4381 *dpy-28(s939)/qC1[qIs26]*, AV106 *spo-11(ok79)/nT1[unc?(n754)let?]*, VC255 *him-17(ok424)*, CB6036 *him-17(e2806)*, and *unc-119(ed3); P_{pie-1}::zhp-3::gfp+ unc-119(+)*. Strains were provided by the *Caenorhabditis* Genetics Centre and by Shohei Mitani at the National Bioresource Project of Japan.

Visible marker meiotic recombination assay. Individual animals of genotype *dpy unc/+ +* and *rtel-1; dpy unc/+ +* were plated and transferred daily for four days. In each of the broods, wild type, Dpy, Unc and Dpy Unc phenotypes were scored. Recombination frequencies were calculated as in (*S2*). Genetic map distance (in

centiMorgans) was calculated as recombination frequency multiplied by 100. For recombination experiments using IR, L4-stage animals were treated with 0, 10 or 75 Gy IR from a 2.14 Gy/min Cs^{137} source prior to plating.

SNP marker meiotic recombination assay. Crossover assays were conducted as in (*S3*) with some modifications. The use of balancers was prohibited due to genetic incompatibility with the *rtel-1* mutation. As a result, blind crosses were conducted. Each of many crosses were transferred daily for three days, after which the parent animals were genotyped through PCR based detection of the *rtel-1* and *dpy-28* deletions. Progeny from the appropriate genotype were then used in subsequent crosses or in the final PCR-based single nucleotide polymorphism detection.

Statistics. The 95% confidence interval for each genetic map distance was determined using bootstrap estimates to calculate recombination frequency (and thereby genetic map distance) 10,000 times and the lowest and highest 2.5% value gave the lower and upper bounds for the 95% confidence interval. To test the difference between wild type and *rtel-1* mutants for the number of chromatids with COs, a Poisson regression on the number of chromatids in each CO category was used. A Fisher's exact test comparing the total number of measured intervals with a CO to the total number of measured intervals without a CO was used to compare the total CO frequency across all snip-SNP intervals on the X chromosome for the various genotypes tested. For the interference analysis, given four SNP intervals and all possible configurations of double COs within the intervals, under no interference, it was expected that half of the double COs would be adjacent and half would be separated. A binomial test of proportions was used to test this hypothesis against the distribution of double COs in the various genotypes. A t-test was used to determine if there was a significant

difference between the number of ZHP-3::GFP foci in wild type versus *rtel-1* mutant nuclei.

Immunofluorescence. RAD-51 immunofluorescence was performed as in (*S4*). For RAD-51 staining on *rad-54*(RNAi) animals, the feeding vector was grown in 50ug/ml ampicillin. After 12 hours, IPTG was added to a final concentration of 4mM and the culture was grown for a further 2 hours. The culture was spotted onto MYOB plates containing 1mM IPTG and 1ug/ml carbinocillin. Plates were incubated at 25 degrees overnight. L4-stage animals were placed on the RNAi plates. RAD-51 foci in the germlines were assessed when the animals were adults. In *rad-54*(RNAi)-treated wild type and *rtel-1* animals, foci were counted in the Z-stack images of 100 RAD-51 positive early to mid-pachytene nuclei. This was done in order to avoid counting earlier nuclei that may not have yet formed meiotic DSBs and later nuclei that may be undergoing apoptosis. In wild type and *rtel-1* mutants with and without IR treatment, RAD-51 foci were counted in 100 early pachytene nuclei that were imaged in Z-stacks. The three-dimensional images were flat-projected in order to obtain images that could be used in the figures. The guinea-pig-anti-ZHP-3 antibody (a kind gift from Needhi Bhalla) was pre-adsorbed against *zhp-3* mutant worms and used under standard conditions (as in (*S4*)) at 1:250. Anti-guinea-pig FITC secondary antibody was used at 1:5000. All images were captured using Deltavision microscopy and images were deconvolved and flat projected using SoftWorx software (Applied Precision).

D loop Recombination assay. For the RecA/SSB D loop unwinding assay, 10 µl reactions contained 1 µM 5'-32P-end-labeled 100mer ssDNA in recombination buffer (25 mM Tris-acetate pH 7.5, 5 mM CaCl2, 2 mM MgCl2, 2 mM ATP, 1 mM DTT, 100 µg/ml BSA). The following were then added sequentially, separated by 5

minute incubations at 37°C: 0.5 μM RecA; RTEL1; 0.2 μM SSB; 0.3 mM supercoiled pPB4.3 DNA. After a further 10 minute incubation the products were deproteinized by the addition of one-fifth volume stop buffer (0.1 M Tris-HCl pH 7.5, 0.1 M MgCl2, 3% SDS and 10 mg/ml proteinase K) with 20 min incubation at 37°C. DNA products were analyzed by 1% agarose gel electrophoresis, dried onto filter paper, visualized by autoradiography and quantified using a Phosphorimager.

For the structural preference of D loop unwinding assay, the synthetic D loop substrate (no overhang) was made by annealing oligonucleotides 1 (5'-GCCAGGGACGGGGTGAACCTGCAGGTGGGCGGCTGCTCATCGTAGGTTAGTATCGACCTATTGGTAGAATTCGGCAGCGTCATGCGACGGC-3'), 2 (5'-GCCGTCGCATGACGCTGCCGAATTCTACCACGCTACTAGGGTGCCTTGCTAGGACATCTTTGCCCACCTGCAGGTTCACCCCGTCCCTGGC-3') and 3 (5'-AAGATGTCCTAGCAAGGCACCCTAGTAGC-3'). The 3' ssDNA invasion with 5' overhang was made by annealing oligonucleotides 1, 2 and 4 (5'-TTAGCCTAGCATGTCCAGTCAGGTACGTCAGATGTCCTAGCAAGGCACCCTAGTAGC-3'). The 5' ssDNA invasion with 3' overhang was made by annealing oligonucleotides 1, 2 and 5 (5'-AAGATGTCCTAGCAAGGCACCCTAGTATTAGCCTAGCATGTCCAGTCAGGTACGTCA-3'). Oligonucleotides were gel-purified by denaturing PAGE and 5'-^{32}P-end-labeled using polynucleotide kinase (NEB) and [γ-^{32}P] ATP and annealing was carried out by heating the DNA molecules for two minutes at 100°C, followed by slow cooling to 25°C in 10 mM Tris$(OAc)_2$ pH 8.0, 10 mM Mg$(OAc)_2$, 50 mM K$(OAc)_2$. D loop complexes were purified by gel electrophoresis.

C. elegans RTEL-1 could not be purified due to its insolubility. Human RTEL1, RAD51 and RPA proteins were purified as published previously (*S4-S6*). For the D

loop unwinding assay, reactions (10 µl) contained 5'-^{32}P-labelled D loop complex (0.5 µM) in recombination buffer to which RAD51 (0.5 µM) was added and incubated at 24°C for 5 min, followed by RPA (0.2 µM) at 24°C for 5 min, and then RTEL1 (40 nM) at 37°C for the indicated times. The products were deproteinized by the addition of one-fifth volume of stop buffer, followed by 20 min incubation at 37°C. DNA products were analyzed by electrophoresis through 8% native PAGE run in TBE buffer at 8 V/cm for 2 h, dried onto filter paper and visualized by autoradiography. Products were quantified using a GE Healthcare Phosphorimager.

Supplementary Text

Additional background information

In wild type *C. elegans*, meiotic recombination occurs most frequently in the chromosomal arm regions, while COs are less common in the chromosome centres (*S7-S9*). We previously reported increases in recombination in two genetic intervals near chromosome centres, *dpy-11* to *unc-42* and *dpy-17* to *unc-36*, in *rtel-1* mutants (*S4*). These data indicate that recombination is increased in some genetic intervals in *rtel-1* mutants. However, at least one *C. elegans* gene mutation has been identified (*rec-1*) that alters recombination distribution, but not overall meiotic CO number (*S2*). It therefore remained possible that like *rec-1*, the increase in recombination in *rtel-1* mutants simply reflected an altered distribution of CO events rather than a global increase in meiotic COs. To distinguish between these two possibilities we measured recombination using visible genetic markers in five genetic intervals on three different chromosomes, including both chromosome centre and arm regions. Crossover recombination was increased in every region in the *rtel-1* mutant, ranging from a 2-fold to 3.5-fold increase over the wild type recombination rate (Figure 1A, Table S1). These data indicate that in *rtel-1* mutants, meiotic recombination is elevated both in chromosome centres and in arm regions, suggesting a breakdown of complete COI in *rtel-1* mutants.

Increased COs in *rtel-1* mutants and the limitations of the snip-SNP assay for recombination

The data generated from the snip-SNP assay for recombination likely underestimates the total number of COs in any genotype because it is based on SNPs at five sites along the chromosome. Because the assay uses individual animals, the amount of DNA available for the assay is limited, and this restricts the

number of SNP sites that can be tested. The SNP markers are distributed along 80% of the chromosome, leaving recombination on 20% of the chromosome unmeasured. Furthermore, double CO events occurring in the same interval between two adjacent SNPs cannot be detected and appear as NCOs. Nevertheless, recombination was significantly increased in *rtel-1* mutants by this assay. Based on our genetic data, recombination was increased at least 2-fold in every interval tested. If extrapolated to the entire genome, this would predict a minimum average of two COs per chromosome and 12 COs per nucleus in *rtel-1* mutants, which is twice the wild type number of one CO per chromosome and six COs per nucleus. Given that the average number of DSBs per chromosome is 2.1 (*S10*), the increase in COs in *rtel-1* mutants is consistent with the hypothesis that all DSBs are converted in COs in the absence of RTEL-1.

Two classes of COs are increased in *rtel-1* mutants

Based on our genetic results, we would expect to see a minimum two-fold increase in ZHP-3 foci in *rtel-1* mutants if ZHP-3 marks all CO events. Eighteen percent of *rtel-1* mutant nuclei contained more than 6 foci, which represents a significant increase over wild type ($p<0.01$). However, the majority of *rtel-1* mutant nuclei contained six foci, and those that had greater than six foci most often had only seven or eight foci (Figure 3C). After 75Gy IR treatment, ZHP-3 foci were unchanged: wild type animals with no IR had 1% of nuclei with greater than 6 foci; wild type animals after IR had 3% of nuclei with greater than 6 foci; *rtel-1* mutants with no IR had 18% of nuclei with greater than 6 foci; *rtel-1* mutants with IR had 17% of nuclei with greater than 6 foci (Figure 3C). However, genetic measurements of CO frequency after IR treatment revealed a large, dose-dependent increase in COs in *rtel-1* mutants. These data indicate that two classes of meiotic CO events are

elevated in *rtel-1* mutants. These two classes may represent (I) obligate-type COs marked by ZHP-3 and (II) additional COs resulting from recombination repair of meiotic DSBs not associated with ZHP-3 in the *rtel-1* mutant.

Excess COs are dependent on the MUS-81 endonuclease

We show that two classes of COs are present in *rtel-1* mutants: one marked by ZHP-3, which may represent the obligate CO class, and a second class that results from recombination repair of meiotic DSBs not associated with ZHP-3. It is possible that the second class of recombination events in *rtel-1* mutants depends on the MUS-81 endonuclease in *C. elegans*, as is the case for class II recombination events in budding yeast (*S11, S12*). This is consistent with our previous observation that *mus-81 rtel-1* double mutants display synthetic embryonic lethality (*S4*). The synthetic lethality of *mus-81 rtel-1* double mutants prevented us from directly testing whether or not the excess crossing over in *rtel-1* mutants is dependent on MUS-81. However, wild type animals that are treated with ionizing radiation to generate extra meiotic DSBs show small to moderate increases in recombination (*S10, S13*) that we reasoned may be similarly dependent on MUS-81. Indeed, using genetic methods to measure recombination between *dpy-11* and *unc-42*, X-ray treated *mus-81* heterozygotes showed a 2.5-fold increase in CO recombination that did not occur in *mus-81* homozygotes (Figure S4). Given that MUS81 processes meiotic recombination intermediates to generate COs (*S14-S16*), these data suggest that MUS-81 is likely required for formation of the second class of ZHP-3 non-associated COs. Furthermore, *mus-81* mutant hatching after X-ray treatment is reduced by 45% compared to a control, suggesting that MUS-81 is important for repair of DSBs in this context.

We used an anti-ZHP-3 antibody to assess ZHP-3 foci in *mus-81 rtel-1* double mutant worms. ZHP-3, the ortholog of budding yeast Zip3, localizes along the length of the synaptonemal complex, the proteinaceous structures that physically attaches homologous chromosomes, where it appears as a string of ZHP-3 in early and mid-pachytene (*S17*). By late pachytene/diplotene, ZHP-3 becomes restricted to foci, with one focus per chromosome normally being observed in wild type. Thus, two phenotypes are visible by ZHP-3 staining: the timing of ZHP-3 restriction to foci and the number of foci formed at late pachytene/diplotene. A large number of ZHP-3 strings (where individual ZHP-3 spots could not be defined) were observed in *mus-81* and *mus-81 rtel-1* double mutants at late pachytene/diplotene, while strings were never observed in wild type nuclei. In *mus-81* mutants, strings of ZHP-3 were observed in 46% of nuclei, while in *mus-81 rtel-1* double mutants, ZHP-3 strings occurred in 65% of nuclei. These data suggest that in *mus-81* and *mus-81 rtel-1* double mutants there is a delay in ZHP-3 restriction to foci, and that this occurs more frequently in the absence of both MUS-81 and RTEL-1. We speculate that the delay in ZHP-3 restriction to foci may be due to delayed or incomplete processing of recombination intermediates in the absence of MUS-81 and RTEL-1; this is consistent with the persistence of RAD-51 foci observed in the *mus-81 rtel-1* double mutant (*S4*). However, in the 35% of *mus-81 rtel-1* double mutant nuclei where ZHP-3 did become restricted to foci, the number of foci was increased (Figure 3D; the mean number of ZHP-3 foci per nucleus for animals of each genotype was as follows: wild type 6.01, *mus-81* 6.06, *rtel-1* 6.23, *mus-81 rtel-1* 6.70). This results suggests that, when CO resolution does occur, excess obligate-type COs are formed in *mus-81 rtel-1* double mutants. Together, the delay in or lack of recombination intermediate processing and the excess obligate-type COs formed when processing

does occur likely account for the synthetic embryonic lethality of *mus-81 rtel-1* double mutants.

A Location of all double and triple crossovers by genotype

rtel-1	Location of Crossovers			
	A-C	C-D	D-E	E-F
Double crossovers		X	X	
		X	X	
		X		X
	X			X
	X		X	
		X		X
			X	X
		X	X	
	X			X
			X	X
		X		X
	X	X		
			X	X
Triple crossovers		X	X	X
	X		X	X

rtel-1; dpy-28/+	Location of Crossovers			
	A-C	C-D	D-E	E-F
Double crossovers		X	X	
	X	X		
		X	X	
			X	X
			X	X
	X		X	
		X	X	
	X			X
	X			X
	X			X
	X	X		
	X			X
		X		X
		X		X
		X		X
			X	X
			X	X
	X			X
			X	X
			X	X
Triple crossovers		X	X	X
		X	X	X
	X	X	X	
	X		X	X
		X	X	X
		X	X	X
	X	X	X	
	X	X	X	
	X		X	X
		X	X	X
	X		X	X
	X		X	X
Quadruple crossovers	X	X	X	X
	X	X	X	X

dpy-28/+	Location of Crossovers			
	A-C	C-D	D-E	E-F
Double crossovers			X	X
			X	X
	X			X
			X	X
		X		X
			X	X
			X	X
	X		X	
			X	X
			X	X
	X			X
			X	X
Triple crossovers	X		X	X
	X		X	X

B

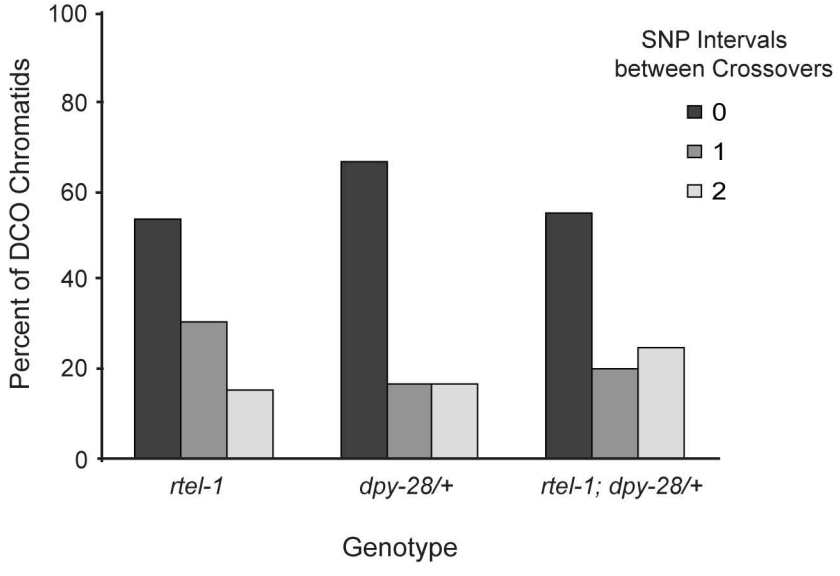

A

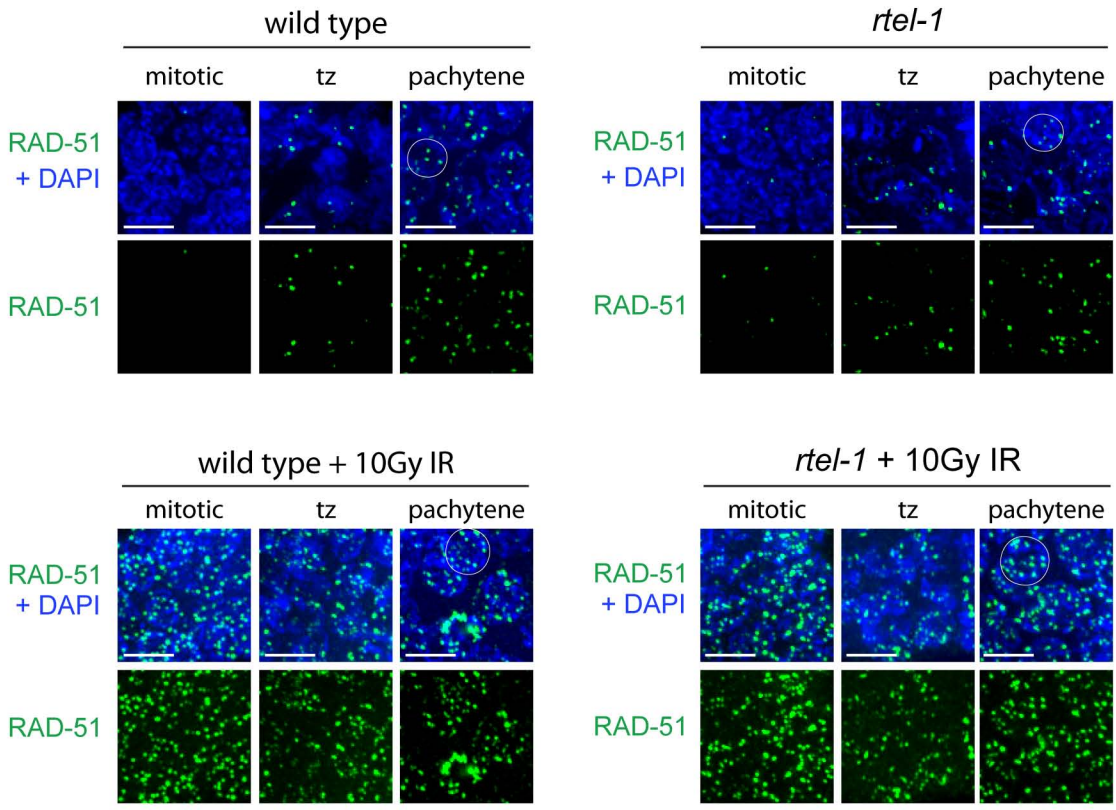

B

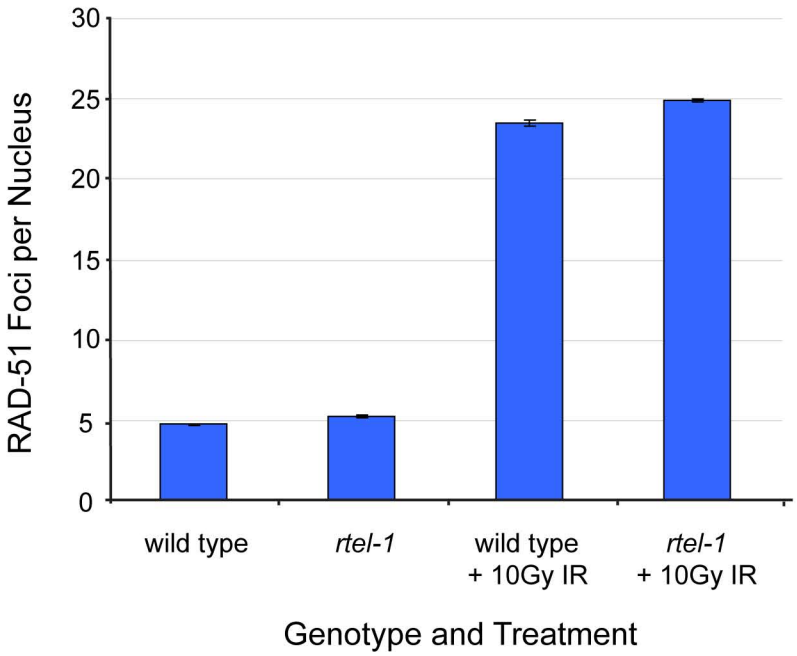

Youds et al. Figure S2.

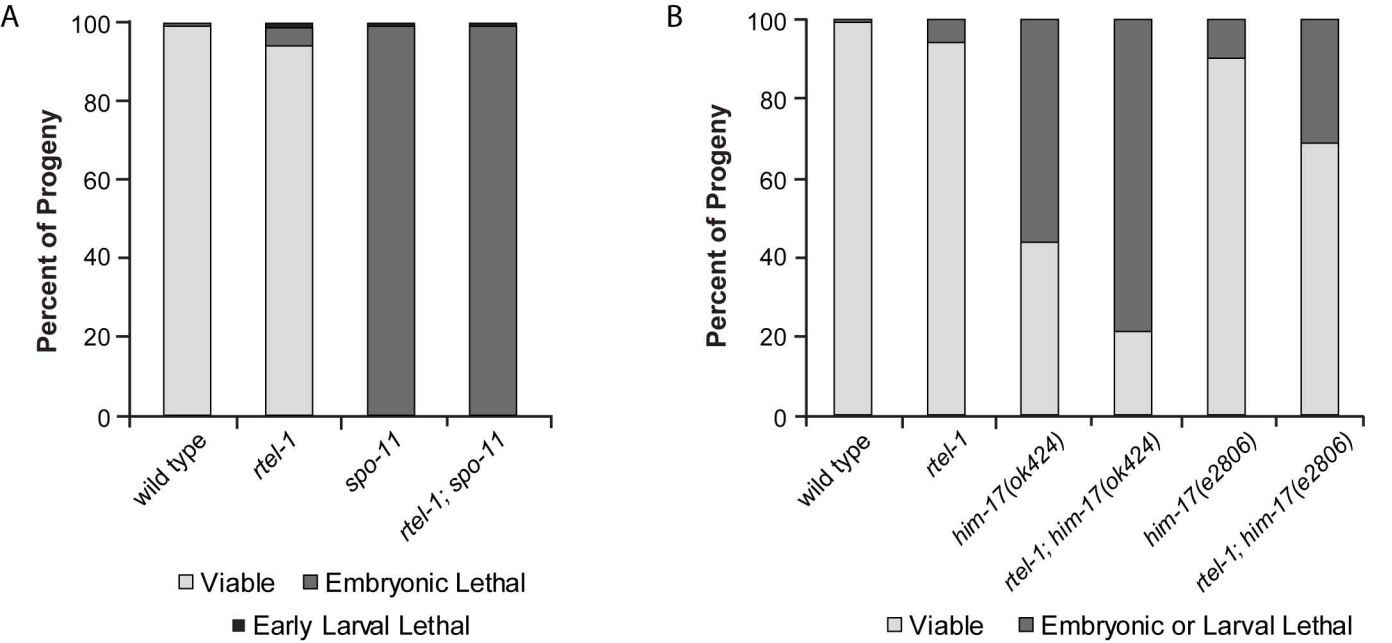

Youds et al. Figure S3.

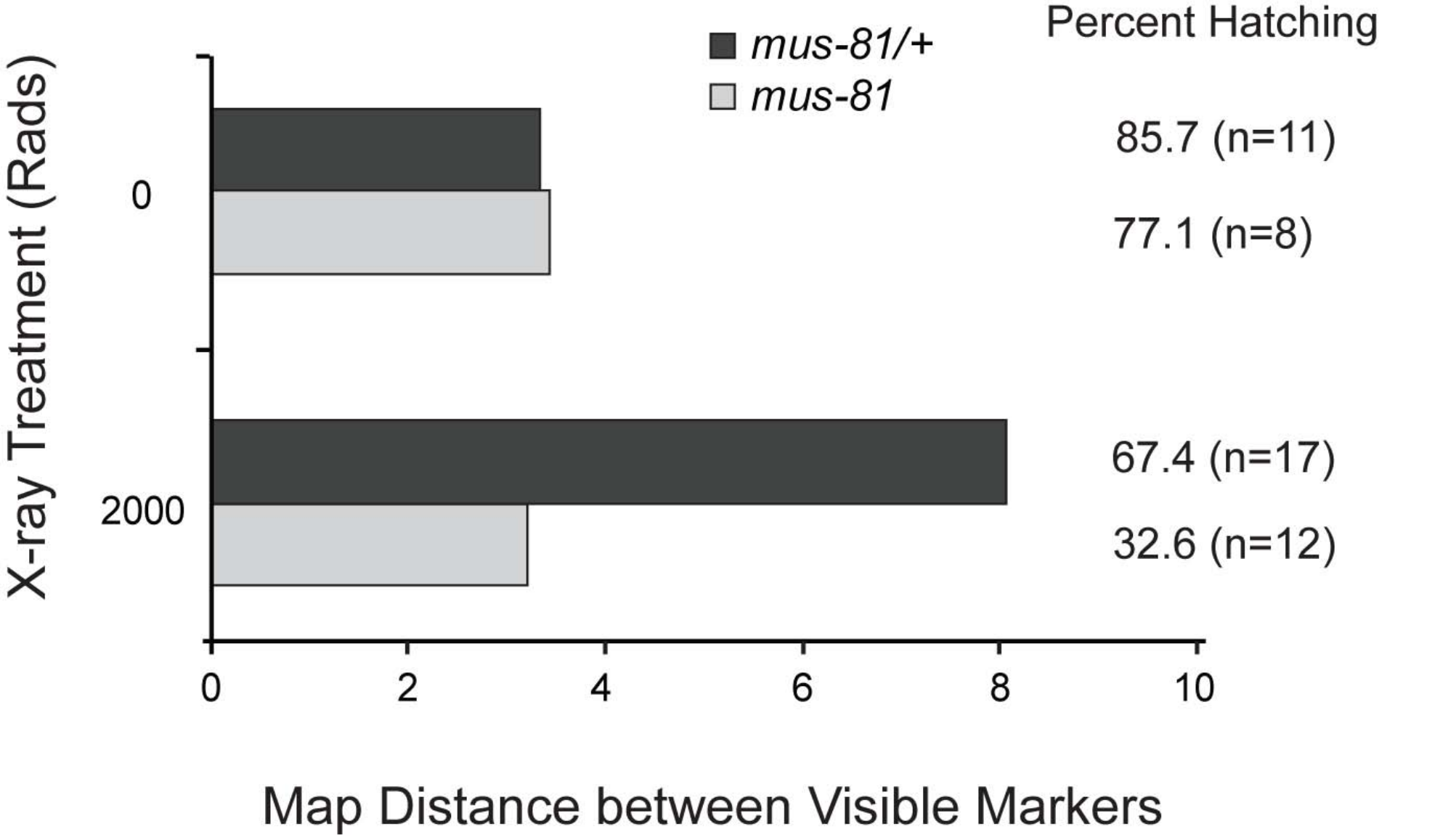

Youds et al. Figure S4

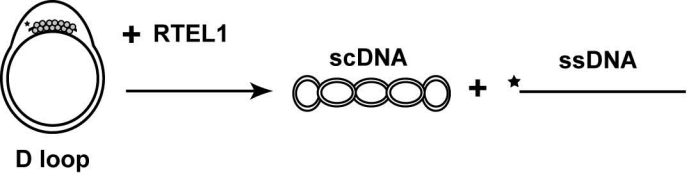

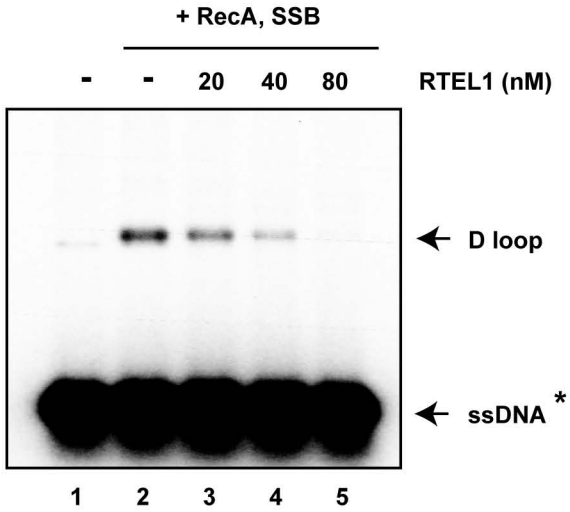

Youds et al. Figure S5

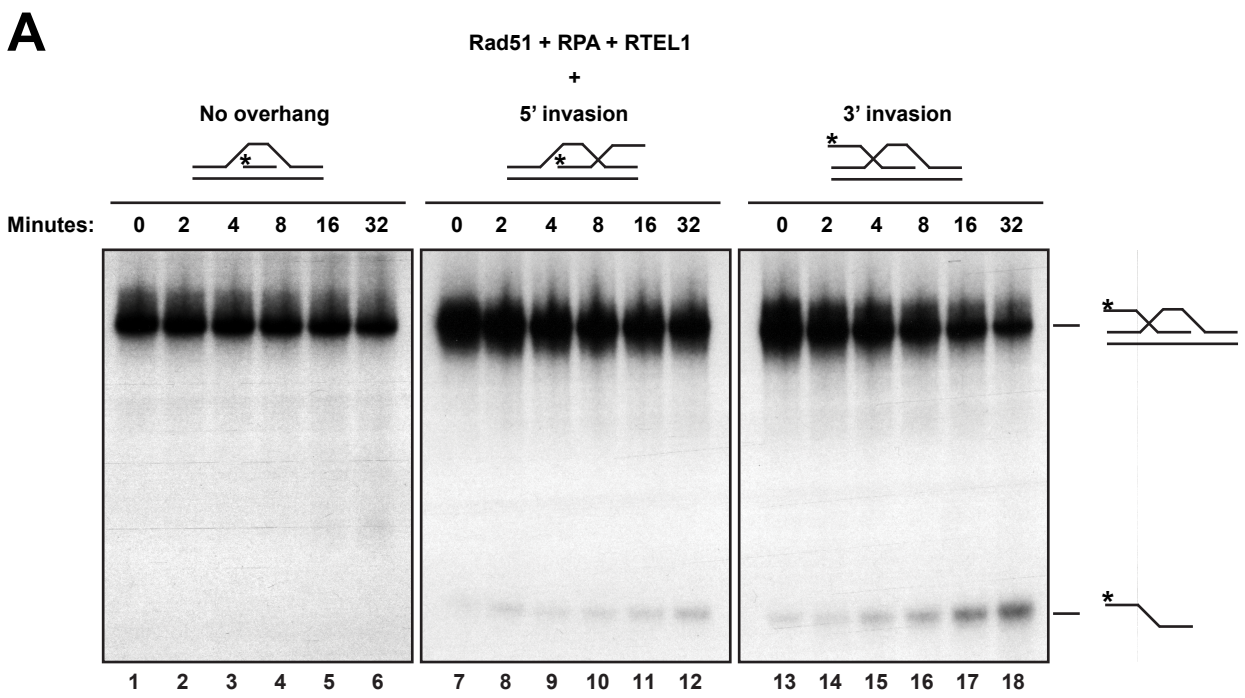

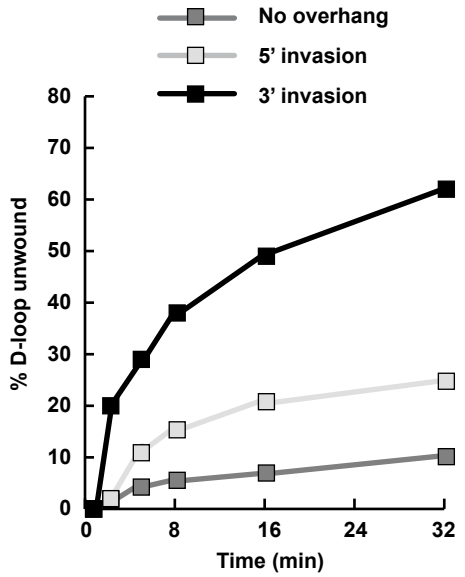

Youds et al. Figure S6

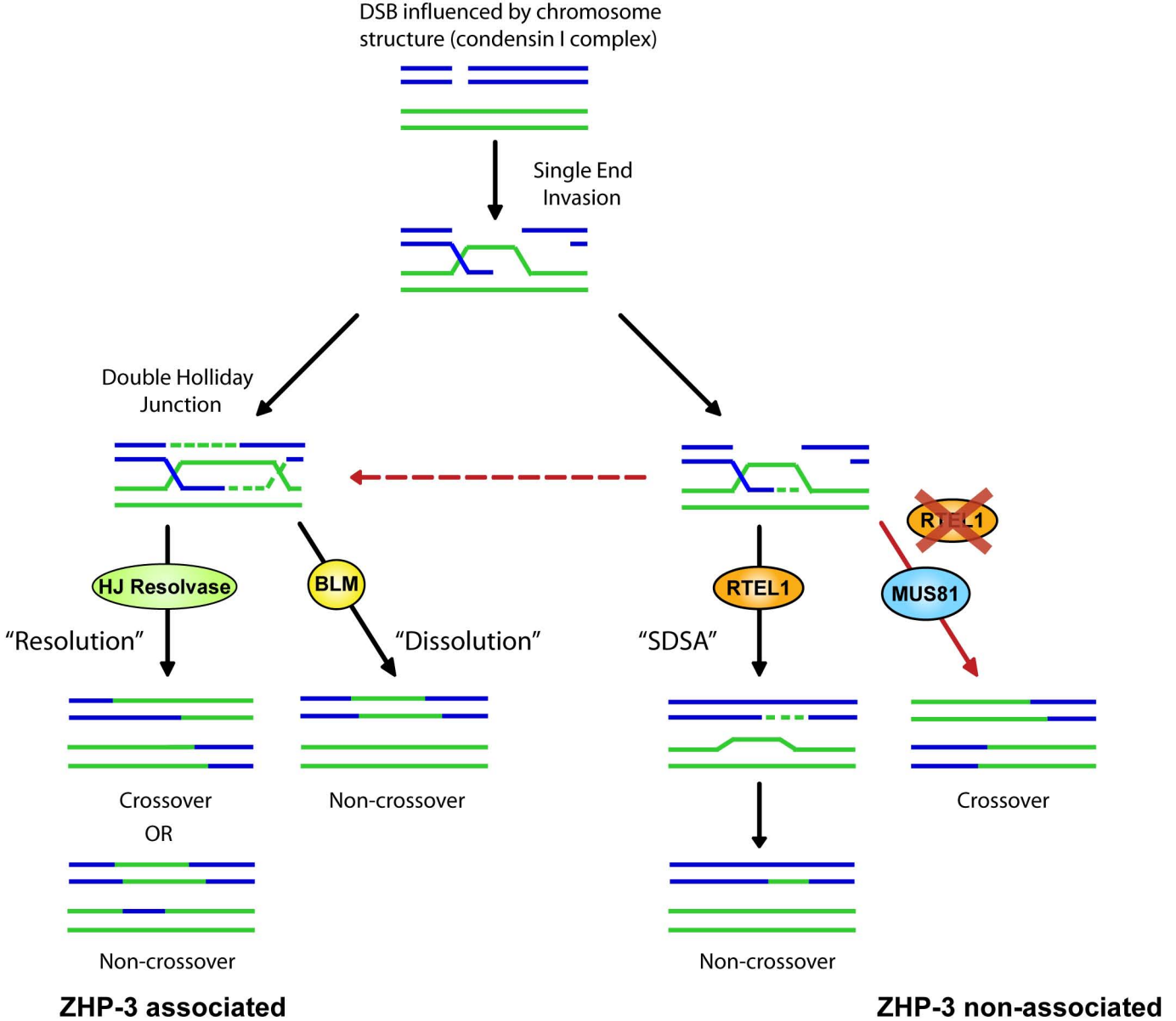

Youds et al. Figure S7.

Figure Legends

Figure S1. CO locations and distribution by genotype. (A) Locations of all double and triple COs observed in the SNP intervals A-C, C-D, D-E and E-F in *rtel-1* and *dpy-28/+* single mutants and in *rtel-1; dpy-28/+* double mutants. Each X represents a CO and each row is an individual chromatid that was tested by snip-SNP analysis. (B) Number of snip-SNP intervals between double-COs for each genotype *rtel-1*, *dpy-28/+* and *rtel-1; dpy-28/+*.

Figure S2. RAD-51 foci in wild type and *rtel-1* mutants without and with IR treatment. (A) Representative flat projected images of RAD-51 (green) and DAPI (blue) in wild type and *rtel-1* mutants with no treatment and 1 hour after 10Gy IR. The zones of the gonad shown are: the mitotic zone, transition zone (tz) and early pachytene. Circles have been drawn around individual pachytene nuclei to aid the reader. Scale bars are 5μm. (B) Counts of RAD-51 foci in 100 Z-stack imaged early pachytene nuclei in wild type and *rtel-1* mutants with no treatment and 1 hour after 10Gy IR. Error bars are SEM.

Figure S3. No rescue of the *spo-11* and *him-17* mutant phenotypes by *rtel-1* mutation. (A) Viability, embryonic and larval lethality in the broods of wild type, *rtel-1*, *spo-11* and *rtel-1; spo-11* double mutants. (C) Viability and lethality in the broods of wild type, *rtel-1*, *him-17* and *rtel-1; him-17* double mutants. *ok424* is a deletion allele of *him-17* and *e2806* is a point mutation.

Figure S4. Excess COs after X-ray treatment are dependent on MUS-81. Recombination as measured by genetic map distance (in centiMorgans) between the visible genetic markers *dpy-11* and *unc-42* in untreated *mus-81/+* and *mus-81* and after 2000Rads X-ray. Progeny survival is reported as percent hatching in the column at right. n is the number of parent animals of which progeny were scored.

Figure S5. RTEL1 disrupts pre-formed D loops generated by RecA/SSB. Shown is a schematic of the D loop disruption assay. D loops preformed by RecA/SSB were incubated with the indicated concentrations of RTEL1 before analysis on agarose gels.

Figure S6. (A) Time course of RTEL1 activity towards different D loop substrates. D loop substrates with no overhang, 5' ssDNA invasion with 3' overhang or 3' ssDNA invasion with 5' overhang were incubated with RTEL1 + Rad51 + RPA for the indicated times. The fastest migrating band corresponds to the displaced radiolabelled ssDNA probe and the slower species represents the D loop substrate. (B) Shown is quantification of the percent D loop unwound over time.

Figure S7. Model for RTEL-1/RTEL1 function in meiotic NCO DSB repair. COs (ZHP-3-associated in *C. elegans*) or NCOs can be generated through resolution of double Holliday junctions by the HJ resolvase. HIM-6/BLM may also promote dissolution of this structure to create a NCO. In the wild type, single end invasion (D loop) intermediates would be dissociated by RTEL-1/RTEL1 to promote SDSA and, thereby, a NCO repair outcome. In the absence of RTEL-1/RTEL1, extra COs are formed either through the formation of more double Holliday junctions (dashed red arrow) or by processing of recombination intermediates by MUS-81/MUS81 (red arrow), which would generate a CO (ZHP-3 non-associated in *C. elegans*).

Interval	Chromosomal Location	Genotype	Total Progeny	Number of Recombinants	Map Distance in cM (95% CI)	Fold Increase over Wild Type
dpy-17 unc-36	**III centre**	**wild type**	2185	26	1.20 (0.77-1.74)	**3.5**
		rtel-1	444	18	4.14 (2.47-6.24)	
dpy-18 unc-25	**III arm**	**wild type**	3483	238	7.08 (6.19-8.02)	**2.0**
		rtel-1	776	100	13.85 (11.05-16.74)	
dpy-11 unc-42	**V centre**	**wild type**	2115	78	3.76 (2.97-4.65)	**2.5**
		rtel-1	659	58	9.23 (6.96-11.98)	
dpy-11 unc-60	**V arm**	**wild type**	4524	472	11.04 (10.05-12.09)	**3.2**
		rtel-1	661	190	34.78 (29.66-40.37)	
unc-1 dpy-7	**X arm**	**wild type**	2683	394	15.96 (14.38-17.57)	**2.1**
		rtel-1	1424	398	33.59 (30.19-37.29)	

Youds et al. Table S1.

Interval	Treatment	Genotype	Total Progeny	Number of Recombinants	Map Distance in cM (95% CI)	Fold increase over untreated wild type
dpy-11 unc-42	**No IR control**	**wild type**	2115	78	3.76 (2.97-4.65)	**1.0**
		rtel-1	659	58	9.23 (6.96-11.98)	**2.5**
	Post 10 Gy IR	**wild type**	2929	120	4.18 (3.44-5.00)	**1.1**
		rtel-1	885	112	13.57 (10.97-16.38)	**3.6**
	Post 75 Gy IR	**wild type**	2732	122	4.57 (3.77–5.42)	**1.2**
		rtel-1	899	136	16.49 (13.74–19.33)	**4.4**
dpy-17 unc-36	**No IR control**	**wild type**	2185	26	1.20 (0.77-1.74)	**1.0**
		rtel-1	444	18	4.14 (2.47-6.24)	**3.5**
	Post 10 Gy IR	**wild type**	2061	24	1.17 (0.73-1.70)	**1.0**
		rtel-1	1289	78	6.24 (4.92-7.75)	**5.2**
	Post 75 Gy IR	**wild type**	2964	74	2.53 (2.00-3.15)	**2.1**
		rtel-1	2142	166	8.07 (6.82-9.37)	**6.7**

Youds et al. Table S2.

Table Legends

Table S1. Meiotic recombination is increased in *rtel-1* mutants in all genetic intervals tested. Interval indicates the two visible markers between which recombination was measured. Map distance is reported in centiMorgans, and the 95% confidence interval for each map distance is reported in brackets.

Table S2. Recombination is further elevated in *rtel-1* mutants after treatment with ionizing radiation (IR). Map distance is reported in centiMorgans, and the 95% confidence interval for each map distance is reported in brackets.

References

S1. S. Brenner, *Genetics* **77**, 71 (May, 1974).
S2. M. C. Zetka, A. M. Rose, *Genetics* **141**, 1339 (Dec, 1995).
S3. C. J. Tsai *et al.*, *Genes Dev* **22**, 194 (Jan 15, 2008).
S4. L. J. Barber *et al.*, *Cell* **135**, 261 (Oct 17, 2008).
S5. P. Baumann, F. E. Benson, N. Hajibagheri, S. C. West, *Mutat Res* **384**, 65 (Aug, 1997).
S6. L. A. Henricksen, C. B. Umbricht, M. S. Wold, *J Biol Chem* **269**, 11121 (Apr 15, 1994).
S7. D. G. Albertson, Rose, A.M., Villeneuve, A.M., in *C. elegans II,* B. T. Riddle DL, Meyer BJ, Priess JR, Ed. (Cold Spring Harbor Laboratory Press, Cold Spring Harbor, NY, 1997).
S8. T. M. Barnes, Y. Kohara, A. Coulson, S. Hekimi, *Genetics* **141**, 159 (Sep, 1995).
S9. M. V. Rockman, L. Kruglyak, *PLoS Genet* **5**, e1000419 (Mar, 2009).
S10. D. G. Mets, B. J. Meyer, *Cell* **139**, 73 (Oct 2, 2009).
S11. D. K. Bishop, D. Zickler, *Cell* **117**, 9 (Apr 2, 2004).
S12. N. M. Hollingsworth, S. J. Brill, *Genes Dev* **18**, 117 (Jan 15, 2004).
S13. J. S. Kim, A. M. Rose, *Genome* **29**, 457 (Jun, 1987).
S14. F. Osman, J. Dixon, C. L. Doe, M. C. Whitby, *Mol Cell* **12**, 761 (Sep, 2003).
S15. M. N. Boddy *et al.*, *Cell* **107**, 537 (Nov 16, 2001).
S16. G. A. Cromie *et al.*, *Cell* **127**, 1167 (Dec 15, 2006).
S17. N. Bhalla, D. J. Wynne, V. Jantsch, A. F. Dernburg, *PLoS Genet* **4**, e1000235 (Oct, 2008).